Supporting Information

Increasing the Collision Rate of Particle Impact Electroanalysis with Magnetically Guided Pt-Decorated Iron Oxide Nanoparticles

*Donald A. Robinson, Jason J. Yoo, Alma D. Castañeda, Radhika Dasari, Brett Gu, Richard M. Crooks, and Keith J. Stevenson**

Department of Chemistry, The University of Texas at Austin, Austin, TX 78712, United States.

*stevenson@cm.utexas.edu

SI Contents **Page #**

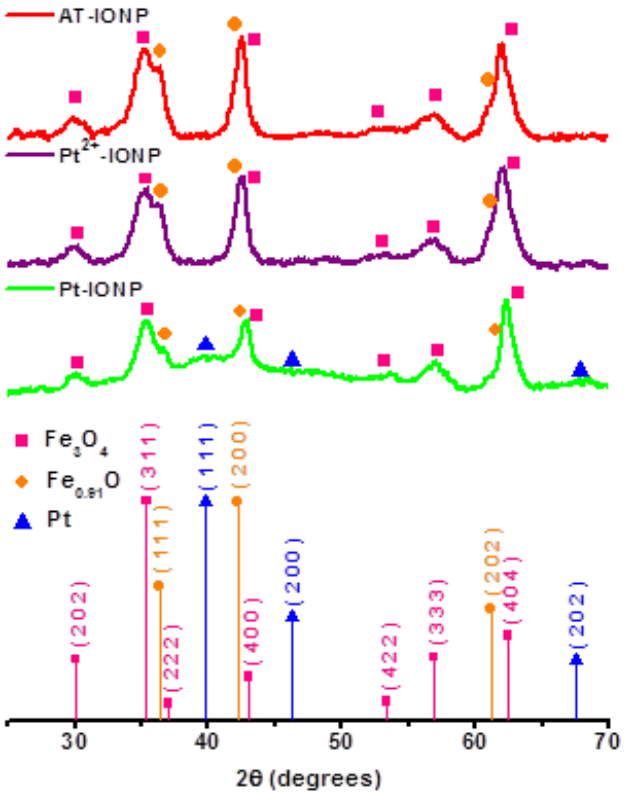

Figure S1. (a) Powder XRD patterns for AT-IONP, Pt^{2+}-IONP, and Pt-IONP along with (b) corresponding diffraction lines for Fe_3O_4, $Fe_{0.91}O$, and Pt.[1–3]

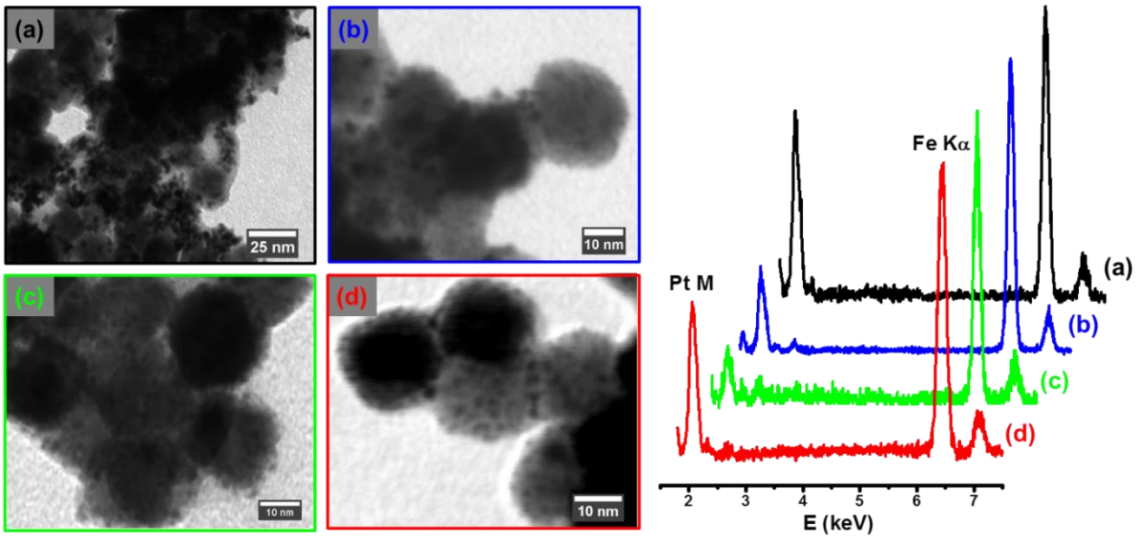

Figure S2. (*left panel*) STEM images and (*right panel*) corresponding EDX spectra for different hybrid Pt-IONP samples synthesized under different reaction conditions: (a) using naked IONPs without hydroxylamine, (b) using naked IONPs with hydroxylamine, (c) using AT-IONPs without hydroxylamine, and (d) using AT-IONPs with hydroxylamine. All EDX spectra were normalized by the Fe K_α peak intensity.

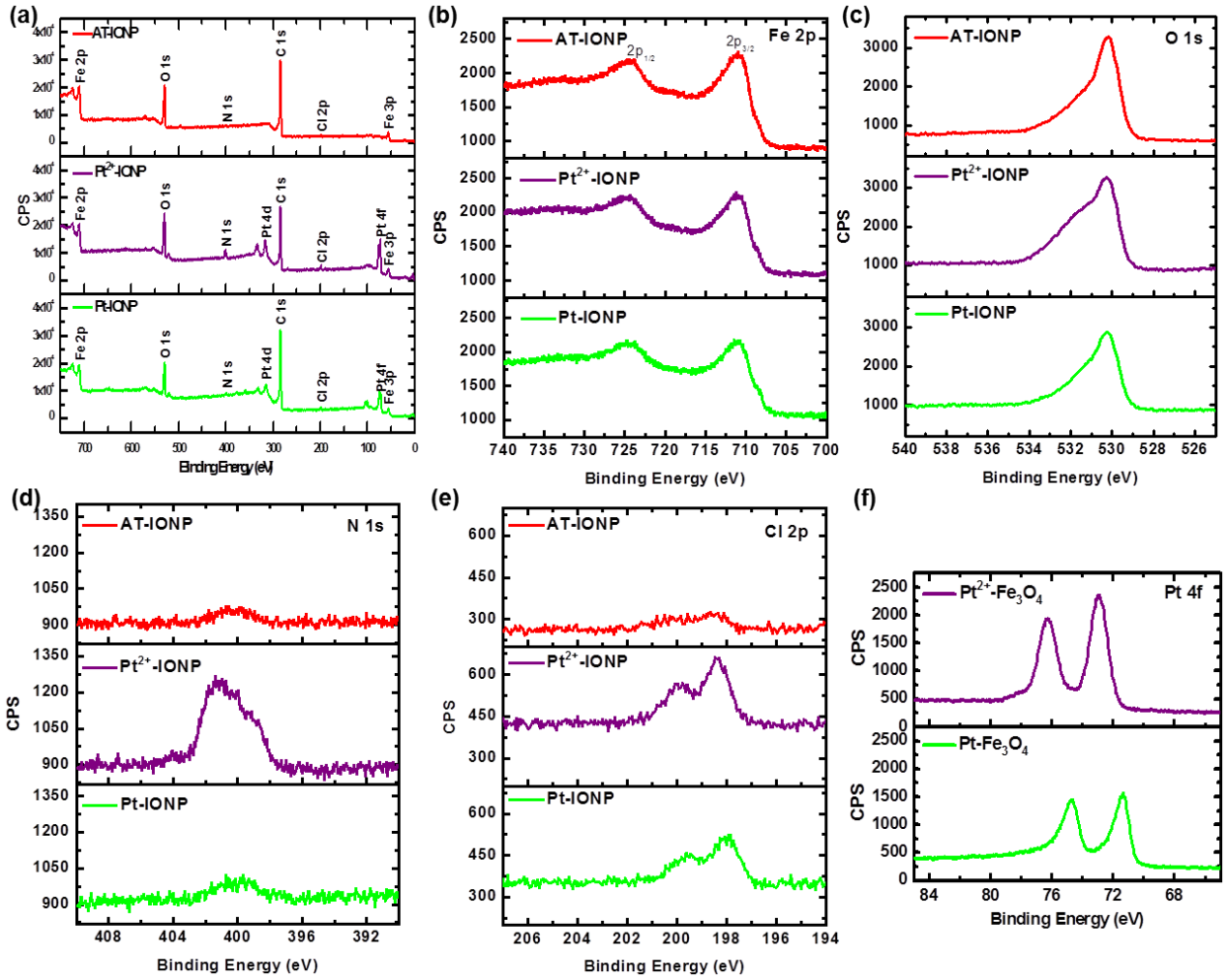

Figure S3. XP spectra for (a) survey region, (b) Fe_{2p}, (c) O_{1s}, (d) N_{1s}, (e) Cl_{2p}, and (f) Pt_{4f} regions for AT-IONP, Pt^{2+}-IONP, and Pt-IONP.

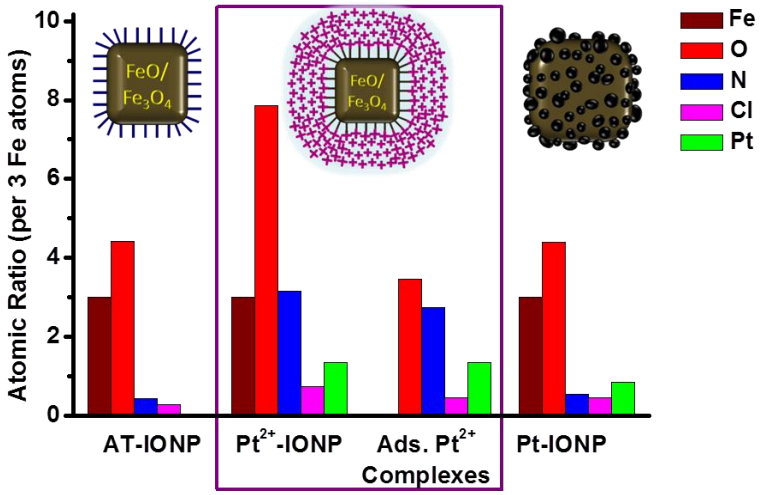

Figure S4. Summary of XPS quantitative analysis with relative elemental composition normalized by Fe atomic % and multiplied by 3 to relate to stoichiometry of Fe_3O_4. The data for the adsorbed species is simply the difference between that of Pt^{2+}-IONP and AT-IONP.

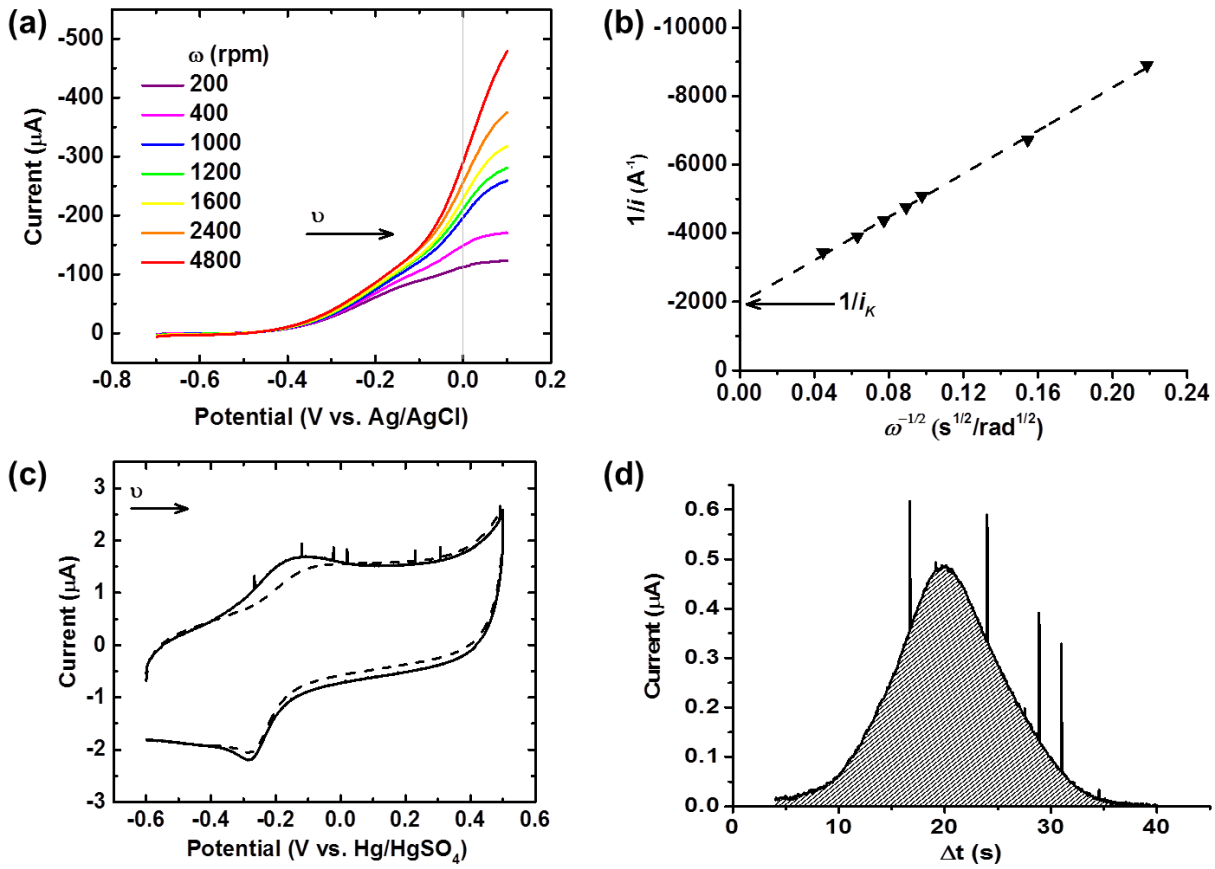

Figure S5: Electrocatalytic activity of Pt-IONPs for hydrazine oxidation: (a) Linear sweep voltammetry (υ = 20 mV/s) at various rotation rates for Pt-IONP catalyst film on GC RDE in the presence of 1.5 mM N_2H_4* and 50 mM SPB, (b) corresponding Koutecky-Levich plot from electrocatalytic current at 0 V vs. Ag/AgCl, (c) cyclic voltammograms of Pt-IONP catalyst film in N_2-purged 0.1 M KOH before (dashed line) and after (solid line) exposure to 650 s of CO bubbling while held at a constant potential of -0.6 V vs $Hg/HgSO_4$, and (d) background corrected CO stripping peak that was integrated to determine Pt ECSA.

*RDE voltammetry of Pt-IONP/C catalyst was performed in 1.5 mM N_2H_4 instead of the 15 mM concentration used later for collision experiments. It was necessary to use a lower concentration of N_2H_4 for RDE experiments in order to avoid excessive N_2 bubble formation. In 15 mM N_2H_4, excessive gas bubbles were observed on the electrode surface and the resulting Koutecky-Levich plot was nonlinear (data not shown).

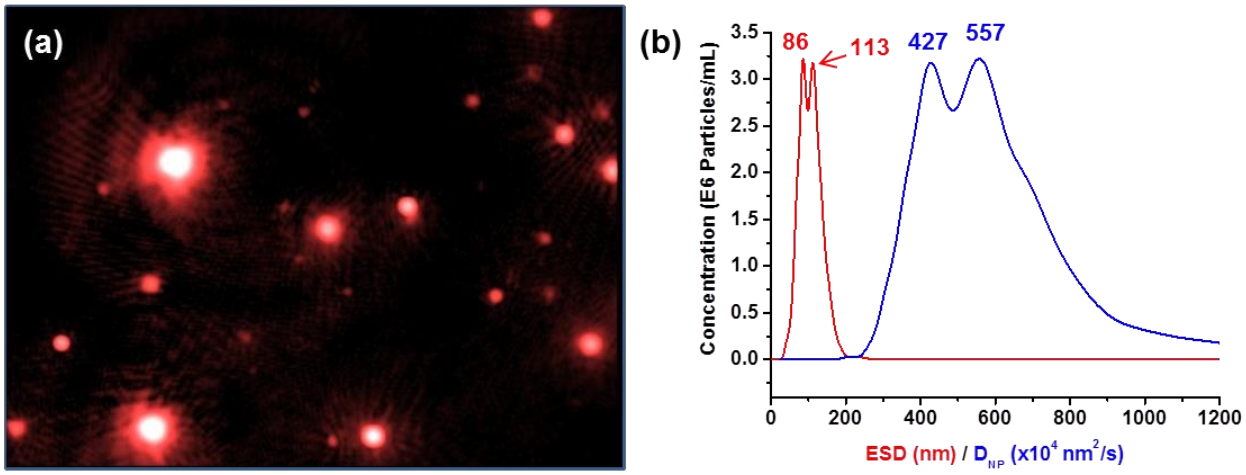

Figure S6. NTA results for a Pt-IONP sample diluted from a stock solution by a factor of 100 in ultra-high purity water to a concentration of 400 fM (by Pt-IONP aggregate): (a) snapshot from video acquired to track NP Brownian motion, (b) nanoparticle diffusion coefficient (D_{NP}) and equivalent spherical diameter (ESD) distributions.

Table S1. Nanoparticle Tracking Analysis Summary for Pt-IONPs

Solution Conditions	**ESD**	D_{NP}	C_{NP}	
	Mean (±s.d.) (nm)	Mean (±s.d.) ($\times 10^{-8}$ cm^2/s)	Diluted Sample ($\times 10^6$ NPs/mL)	Stock (pM)
Pure water	110 (±30)	4 (±2)	240	40.
50 mM SPB	110 (±40)	4 (±2)	310	51
50 mM SPB + 15 mM N_2H_4	110 (±40)	4 (±2)	240	$^{\Psi}$40.

$^{\Psi}$Stock Pt-IONP concentration for EA

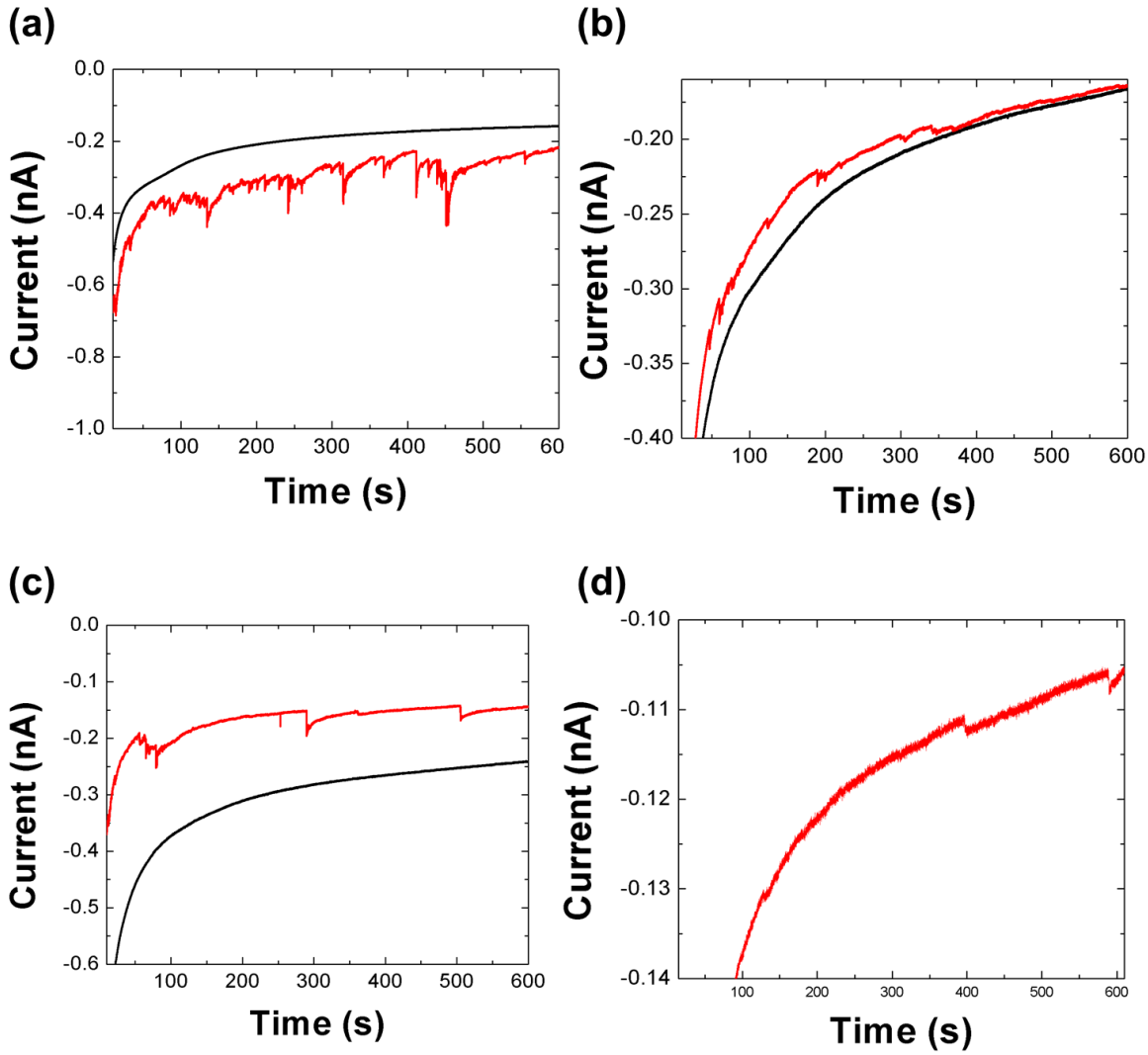

Figure S7: Chronoamperometry of Pt-IONP collisions in microfluidic device without the application of a magnetic field in the presence of 15 mM N_2H_4 in 50 mM SPB (pH 7.5). Black traces correspond to control scan without any Pt-IONPs added and red traces refer to Pt-IONP concentrations of (a) 702 fM, (b) 280 fM, (c) 140 fM, and (d) 57 fM.

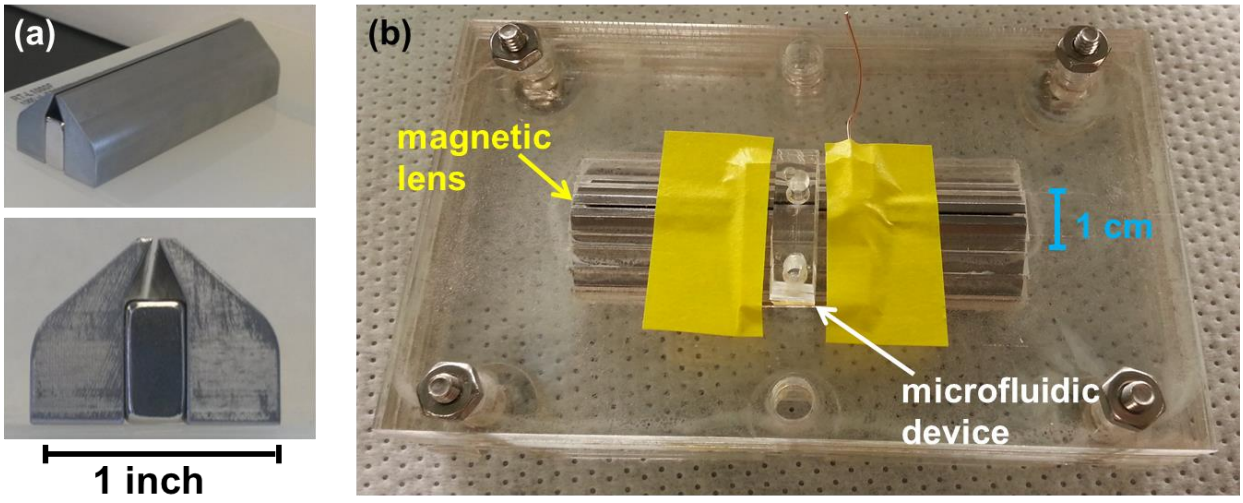

Figure S8: Photographs of (a) magnetic lens and (b) microfluidic device sitting atop the magnetic lens.

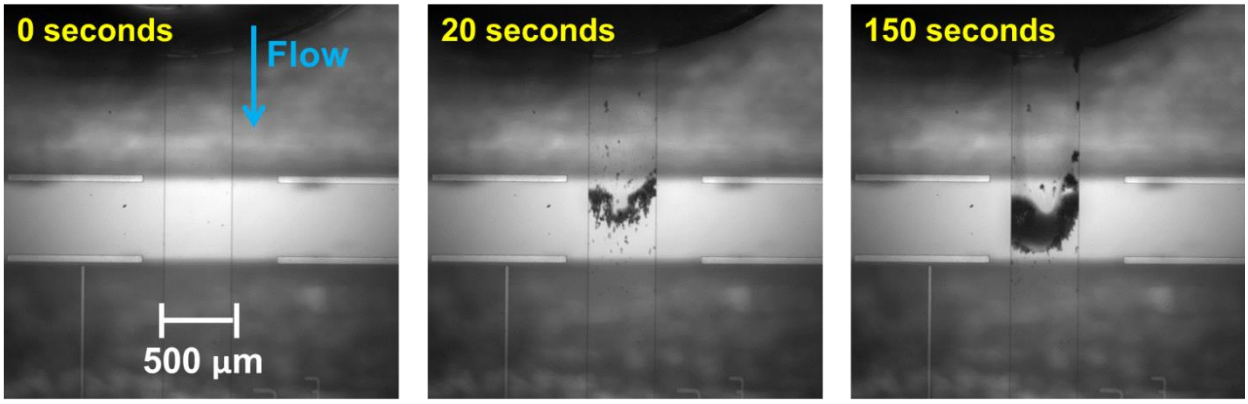

Figure S9: Photographs of Pt-IONP accumulation resulting from attraction to the magnetic lens. The channel width is 500 µm and the Pt-IONP concentration is 40 pM. Gravity-driven flow was accomplished by adding 60 µL of solution in the inlet and 20 µL in the outlet.

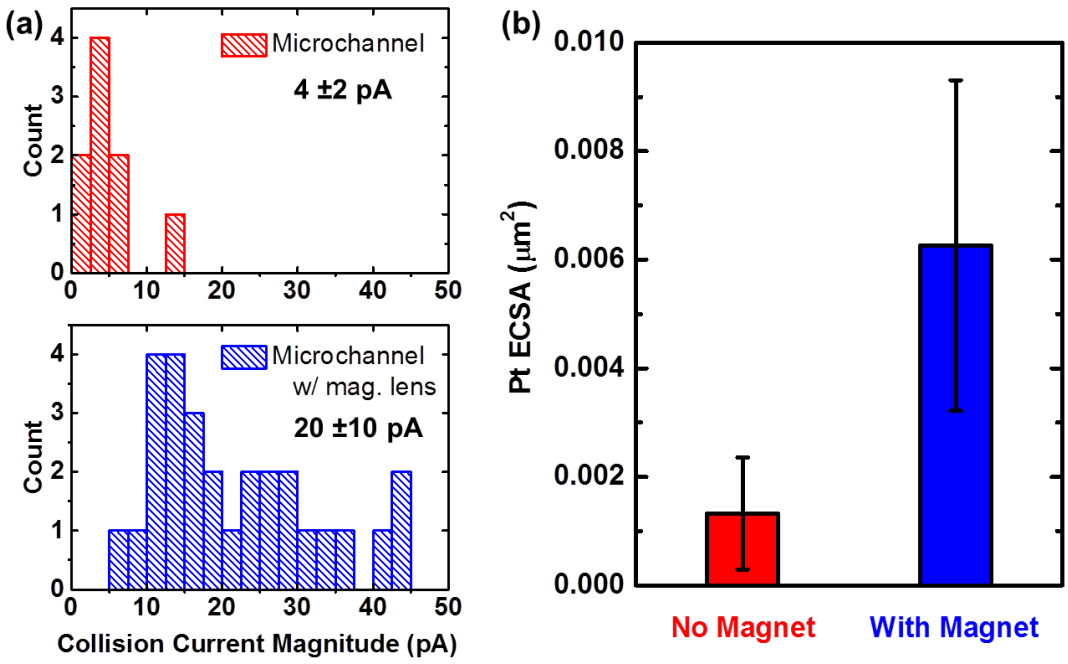

Figure S10: (a) Histograms of EA collision current magnitudes and (b) corresponding average Pt ECSA for particle impact experiments of 60 fM Pt-IONPs in 15 mM N_2H_4* and 50 mM SPB (pH 7.5) with and without the magnetic lens applied.

*Recall that the Pt specific activity in the presence of 1.5 mM N_2H_4 in 50 mM SPB was found to be 34.9 mA/cm^2. Assuming the Pt activity is directly proportional to N_2H_4 concentration, the Pt specific activity in 15 mM N_2H_4 was therefore approximated as 350 mA/cm^2 (due to 10-fold increase in N_2H_4 concentration). The Pt ECSA values presented in Figure S10b were estimated by dividing the averaged data shown in Figure S10a by 350 mA/cm^2.

REFERENCES

(1) Grazulis, S.; Chateigner, D.; Downs, R. T.; Yokochi, A. F. T.; Quiros, M.; Lutterotti, L.; Manakova, E.; Butkus, J.; Moeck, P.; Le Bail, A. Crystallography Open Database - An Open-Access Collection of Crystal Structures. *J. Appl. Crystallogr.* **2009**, *42*, 726–729.

(2) Gražulis, S.; Daškevič, A.; Merkys, A.; Chateigner, D.; Lutterotti, L.; Quirós, M.; Serebryanaya, N. R.; Moeck, P.; Downs, R. T.; Le Bail, A. Crystallography Open Database (COD): An Open-Access Collection of Crystal Structures and Platform for World-Wide Collaboration. *Nucleic Acids Res.* **2012**, *40*, D420–D427.

(3) Downs, R. T.; Hall-Wallace, M. The American Mineralogist Crystal Structure Database. *Am. Mineral.* **2003**, *88*, 247–250.